Urania
Jurnal Ilmiah Daur Bahan Bakar Nuklir

Beranda jurnal: https://ejournal.brin.go.id/urania/

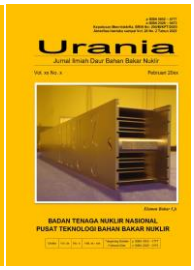

ENHANCING CORROSION RESISTANCE OF AISI–1010 IN RSG–GAS SECONDARY COOLING PIPES THROUGH INHIBITOR COMPOUND INTERVENTION

Enung Nurlia[1], Rahayu Kusumastuti[2], Abdul Aziz[3], Maman Kartaman Ajiriyanto[1], Rosika Kriswarini[1],Gadang Priyotomo[2], Arini Nikitasari[2], Geni Rina Sunaryo[4], Setyo Budi Utomo[3], Sriyono[4], Supriyadi[5], Siska Prifiharni[2], Siti Musabikha[2]
[1]Research Center for Nuclear Material and Radioactive Waste Technology – BRIN
Kawasan Sains dan Teknologi B.J Habibie, Serpong, Tangerang Selatan, Banten 15314
[2]Research Center for Metallurgy – BRIN
Kawasan Sains dan Teknologi B.J Habibie, Serpong, Tangerang Selatan, Banten 15314.
[3]Directorate of Nuclear Facility Management – BRIN
Kawasan Sains dan Teknologi B.J Habibie, Serpong, Tangerang Selatan, Banten 15314
[4]Research Center for Nuclear Reactor Technology – BRIN
Kawasan Sains dan Teknologi B.J Habibie, Tangerang Selatan, Banten 15314
[5]PT. Pertamina (Persero), Indonesia
Jl. Medan Merdeka Timur No. 11-13, Jakarta Pusat, DKI Jakarta 10110
Email: raha006@brin.go.id

(Submitted: 19–11–2024, Revised: 04–01–2025, Accepted: 11–01–2025)

ABSTRACT

ENHANCING CORROSION RESISTANCE OF AISI–1010 IN RSG–GAS SECONDARY COOLING PIPES THROUGH INHIBITOR COMPOUND INTERVENTION. The secondary cooling pipes of RSG-GAS utilize AISI-1010, facilitating water circulation directed to the cooling tower after heat absorption from the primary coolant in the heat exchanger. The subsequent dissipation of heat through the cooling tower into the ambient air aims to uphold the primary coolant's temperature below 40°C. This study focuses on evaluating the impact of inhibitor compounds on the corrosion behavior of AISI 1010. Employing FTIR and GCMS techniques, the inhibitor compounds were analyzed, complemented by visual and SEM examinations for surface morphology. The corrosion rate, influenced by the inhibitor, was quantified using a potentiostat. FTIR analysis revealed a spectrum of functional groups, encompassing O-H, N-H, aromatic compounds, C=O, C-O, and phosphate. Nitrogen, oxygen, and phosphorus elements within the inhibitor exhibited binding interactions with iron in the material. GCMS identified prominent compounds like 1H-Benzotriazole (RTs 14.4469 & 14.7746) - which is a major corrosion inhibitor indicated by its high peak and area percentage, Trans-1-methyl-2-nonyl-cyclohexane (RT 6.6834) as primary constituents of the inhibitor. Visual inspection post-immersion in a 150-ppm inhibitor solution showcased a lack of corrosion products on AISI 1010, contrasting with visible corrosion on the material without an inhibitor. SEM analysis confirmed a protective layer formation. The addition of the inhibitor at 150 ppm significantly enhanced AISI 1010's corrosion resistance, evidenced by a 46.71% reduction in the corrosion rate. This underscores the efficacy of the inhibitor in mitigating corrosion effects on AISI 1010, contributing valuable insights for materials in similar cooling system applications.

Keywords: Secondary cooling pipes, inhibitors, corrosion behavior, RSG-GAS.

INTRODUCTION

The Multipurpose Research Reactor G.A Siwabessy (RSG-GAS) was constructed starting in 1983, achieving its first critical milestone in July 1987 and subsequently inaugurated by the President of Indonesia on August 20, 1987 [1]. RSG-GAS boasts a maximum thermal power of 30 MW and an average neutron flux of 10^{14} $n/cm^2.s^{-1}$ originating from fission reactions [2] This reactor incorporates two cooling systems: the primary and secondary cooling systems, both utilizing water as the cooling fluid. Demineralized water in the primary cooling system functions as a coolant for the reactor, neutron moderator, and thermal neutron shield [3],[4],[5].

RSG-GAS is categorized as a material testing reactor (MTR). Due to its high neutron flux, the core of RSG-GAS is utilized to produce radioisotopes, irradiation of power reactor fuel elements, neutron activation analysis, and non-destructive testing [6].The design of RSG-GAS incorporates low-enriched fuel (19.75%) to mitigate the risk of nuclear fuel proliferation or diversion towards nuclear weapons [7],[8],[9],[10]. However, the low-enriched fuel design poses challenges, as resulting in either a too-short or too-long cycle life for fuel in plate-type research reactor cores like RSG-GAS. This circumstance adversely affects the reactor's effectiveness and efficiency during operation, decreasing its economic viability [11],[12],[13],[14].

The construction of the RSG-GAS plays a critical role in the overall efficiency and safety of the nuclear power plant. One of the key components of the RSG-GAS design is its integration with the secondary cooling system. The secondary cooling pipe connects the RSG-GAS to the cooling loop, allowing heat transfer from the reactor core to the secondary circuit. The design of the secondary cooling pipe must ensure minimal heat loss, durability, and resistance to corrosion under high-temperature and high-pressure conditions. Detailed engineering of the pipe and its integration with the RSG-GAS ensures seamless heat exchange, which is fundamental to the operational stability and safety of the plant.

The secondary cooling pipes of RSG-GAS are constructed from AISI-1010 material [3]. However, other materials, such as AISI-304 and AISI-316, are also commonly used for secondary cooling pipes due to their corrosion resistance and mechanical properties. AISI-304, for example, is favored for its resistance to oxidation and corrosion in many industrial applications, while AISI-316 offers superior corrosion resistance, especially in chloride environments. Despite these alternatives, AISI-1010 is chosen for its cost-effectiveness, availability, and sufficient mechanical properties to withstand the operating conditions within the reactor cooling system. The movement of water within these secondary pipes is directed towards the cooling tower following the absorption of heat from the primary coolant in the heat exchanger [10],[13],[15]. Subsequently, the heat contained in the secondary coolant is dissipated through the cooling tower into the ambient air surrounding the reactor. This process maintains the temperature of the primary coolant below 40°C [9],[16].

Ensuring nuclear reactor safety is paramount, with specific attention directed towards the secondary cooling system [11],[15]. The open recirculation system employed in the RSG-GAS facilitate sample opportunities for oxygen ingress, leading to potential interactions with secondary cooling components [7],[15]. Consequently, mitigating the corrosion of process materials in this environment presents a significant challenge [8],[11]. Although corrosion is an inevitable process, its rate can be managed through a range of strategies, such as meticulous material selection, chemical treatment, coating application, cathodic protection, and anodic protection [8],[17],[18]. Among these corrosion control methods, chemical treatment stands out, particularly through the addition of inhibitors—chemicals designed to reduce corrosion rates by forming a protective passive film [19],[20],[21],[22].

Inhibitors can be classified into three types: cathodic, anodic, and adsorption inhibitors [23],[24],[25]. Anodic inhibitors adsorb on the anodic portion, forming a passive film to protect metals from corrosion, while cathodic inhibitors influence cathodic reactions [26],[27]. Absorption inhibitors, subdivided into organic and inorganic inhibitors, form layers on material surfaces. various treatments have been applied, such as the addition of scale corrosion inhibitors, bioxide and nonbioxide inhibitors, and sulfuric acid to control pH within the range of 6.5 to

 DOI: https://doi.org/10.55981/Urania.2025.8674

8.5 [3]. Siskem, an industrial inhibitor brand, is currently integrated into the secondary cooling system for the stated purposes.

Previous studies have explored the impact of Nalco, an inhibitor, on the corrosion rate of the secondary cooling system. Concentration optimizations have been suggested, such as 100 ppm according to Diyah EL [28]. Sofia's research further indicated an effective concentration of 35% for the inhibitor [29]. In this context, the siskem inhibitor, chosen for its economic feasibility and comparable performance to Nalco, underwent investigation . This research aimed to identify active compounds in the siskem corrosion inhibitor using Fourier Transform Infrared Spectroscopy (FTIR) and Gas Chromatography-Mass Spectrometry (GCMS) assessing its efficiency when applied to AISI-1010 material in the RSG GAS secondary cooling system.

Siskem corrosion inhibitors may contain compounds like phosphate and nitrate, functioning to prevent corrosion and scale formation. Phosphate, binding to Fe on the base metal, forms $FePO_4$ with covalent bonds, creating a protective layer against oxygen attack. The study sought to understand the composition of compounds in the siskem corrosion inhibitor and its impact on the corrosion rate in the RSG-GAS secondary cooling system. Experimental measurements, varying inhibitor concentrations (0 ppm, 50 ppm, 100 ppm, and 150 ppm), were conducted to determine the corrosion rate.

METHODOLOGY

Specimen and Solution Preparation

The materials used in this study included AISI-1010 carbon steel, sourced as the secondary cooling pipe material for the RSG-GAS reactor. The AISI-1010 specimens were cut into cylindrical plates of 1.6 cm in diameter and 0.3 cm in thickness. The specimens were polished using sandpaper 400, 800, 1200 mesh to remove any surface oxides and to achieve a smooth surface. After polishing, the specimens were cleaned with distilled water and dried. The prepared specimens were stored in a desiccator until use. For the immersion tests, raw water sourced from the secondary cooling system of RSG-GAS was used as the corrosive medium, that the raw water composition is 147 µS/cm conductivity, 0.04 ppm Fe, 5 ppm $SO4^{2-}$, 23 ppm silica HR, 23 ppm P reactive, 9 ppm Cl^{-}, 32 ppm Ca, 24 ppm SiO_2 [5]. The corrosion inhibitor solutions were prepared at different concentrations (0 ppm, 75 ppm, 100 ppm, and 150 ppm) using the raw water as the solvent.

Corrosion Inhibitor Preparation

The corrosion inhibitor used in this study was Siskem, an industrial inhibitor brand chosen for its economic feasibility and performance. The inhibitor was prepared by dissolving the required amount in distilled water to achieve different concentrations: 0 ppm, 75 ppm, 100 ppm, and 150 ppm. The solution was stirred thoroughly to ensure homogeneity. The prepared inhibitor solutions were stored in airtight containers to prevent contamination and degradation. Fourier Transform Infrared Spectroscopy was employed to identify the functional groups present in the inhibitor compounds. The FTIR spectra were recorded in the range of 4000–500 cm^{-1}. The GCMS was utilized to analyze the chemical composition of the corrosion inhibitor. The GCMS analysis involved injecting a 1 µL sample into the system, with n-hexane as the preparation medium and helium gas as the carrier. The analysis was performed in qualitative mode, with the chromatography parameters set as follows: column temperature of 250°C, 30 m long HP-5MS column, helium carrier gas flow rate of 1 mL/min, and retention time of 5.2 minutes. The mass spectrometry parameters included electron ionization mode (EI), mass range of 50–550 m/z, and ion abundance detection in the full scan mode.

Surface Analysis

The surface morphology of the AISI-1010 specimens was analyzed using Scanning Electron Microscopy (SEM), Models include the JSM-IT710HR. SEM analysis was conducted on specimens before and after immersion in the inhibitor solutions. The SEM images were taken at magnifications of 100X and 500X to observe the surface features and the formation of any protective layers. include the JSM-IT710HR. SEM analysis was conducted on specimens before and after immersion in the inhibitor solutions. The SEM images were taken at magnifications of 100X and 500X to observe the surface features and the formation of any protective layers.

Electrochemical Test

The corrosion behavior of AISI-1010 in the presence of the corrosion inhibitor was evaluated using electrochemical tests. The tests were conducted using an EG&G Potentiostat/Galvanostat Model 273. The corrosion rate was determined using Tafel polarization measurements. The polarization was performed over a potential range of -250 mV to +250 mV vs. open circuit potential, with a scan rate of 1 mV/s. These parameters ensure that the resulting PDP (Polarization Resistance) curve is consistent with the test conditions. The electrochemical tests were conducted using several techniques, including Open Circuit Potential (OCP), Electrochemical Impedance Spectroscopy (EIS), and Potentiodynamic Polarization (PDP). OCP was used to measure the corrosion potential of the material under open circuit conditions. EIS was employed to evaluate the impedance response and corrosion resistance over a range of frequencies. The corrosion rate was determined using PDP measurements, which involved scanning the potential in a controlled manner to obtain the polarization curve. The AISI-1010 specimens were immersed in the inhibitor solutions at different concentrations (0 ppm, 75 ppm, 100 ppm, and 150 ppm) and the corrosion potential (E_{corr}) and corrosion current density (I_{corr}) were measured. The corrosion rate was calculated based on the Tafel extrapolation method. The experimental setup followed ASTM G3-89 standards for sample preparation and test procedures. The tests were conducted at room temperature to simulate the actual operating conditions of the secondary cooling system. The results were used to evaluate the efficiency of the corrosion inhibitor in reducing the corrosion rate of AISI-1010. The results were used to evaluate the efficiency of the corrosion inhibitor in reducing the corrosion rate of AISI-1010. The efficiency of the corrosion inhibitor was calculated using the equation (1).

$$E(\%) = \frac{CR\ non.Inh - CR\ Inh}{CR\ non.Inh}\ x\ 100 \qquad (1)$$

where CR *non Inh* and CR Inhibitor represent the corrosion rates of AISI-1010 without and with the addition of the corrosion inhibitor, respectively. This formula quantifies the percentage reduction in corrosion rate attributed to the inhibitor's performance.

The Langmuir adsorption isotherm equation was used to evaluate the adsorption behavior of the inhibitor molecules on the surface of AISI-1010. The calculation is expressed as equation (2).

$$\frac{C}{\theta} = \frac{1}{K\ ads} + C \qquad (2)$$

Where C is the concentration of the inhibitor in the solution (ppm), θ is the surface coverage of the inhibitor on the metal, and K_{ads} is the adsorption equilibrium constant, which indicates the strength of the adsorption process. To determine the free energy of adsorption(ΔG_{ads}), the relationship is written in equation (3).

$$\Delta G_{ads} = -\ RT\ \ln K_{ads} \qquad (3)$$

Where R is the universal gas constant (8.314 J/mol.K), and T is the absolute temperature (K). This equation provides insights into the nature of the adsorption process:

a. ΔG_{ads} value less negative than −20 kJ/mol, suggests physisorption,
b. ΔG_{ads} value between −20 kJ/mol and −40 kJ/mol indicates a mixed mechanism of physisorption and
c. ΔG_{ads} value more negative than −40 kJ/mol points to chemisorption involving stronger chemical bonds.

RESULT AND DISCUSSION

FTIR Analysis

FTIR spectroscopic analysis relies on the distinctive features of functional groups present in corrosion inhibitors. The FTIR spectra of the inhibitor samples were acquired using the Shimadzu FTIR model, spanning the IR region with a frequency range of 4000 – 500 cm^{-1} is shown in Figure 1.

Chemical composition of RSG-GAS secondary pipe

The examination of the chemical composition present in the carbon steel material utilized as the secondary cooling pipe material in the RSG-GAS has been systematically conducted in the metallurgy and materials laboratory at Universitas Indonesia, as outlined in Table 1. The carbon steel, specifically AISI 1010, demonstrates a notably low carbon content, thereby classifying it as possessing low strength yet high ductility.

 DOI: https://doi.org/10.55981/Urania.2025.8674

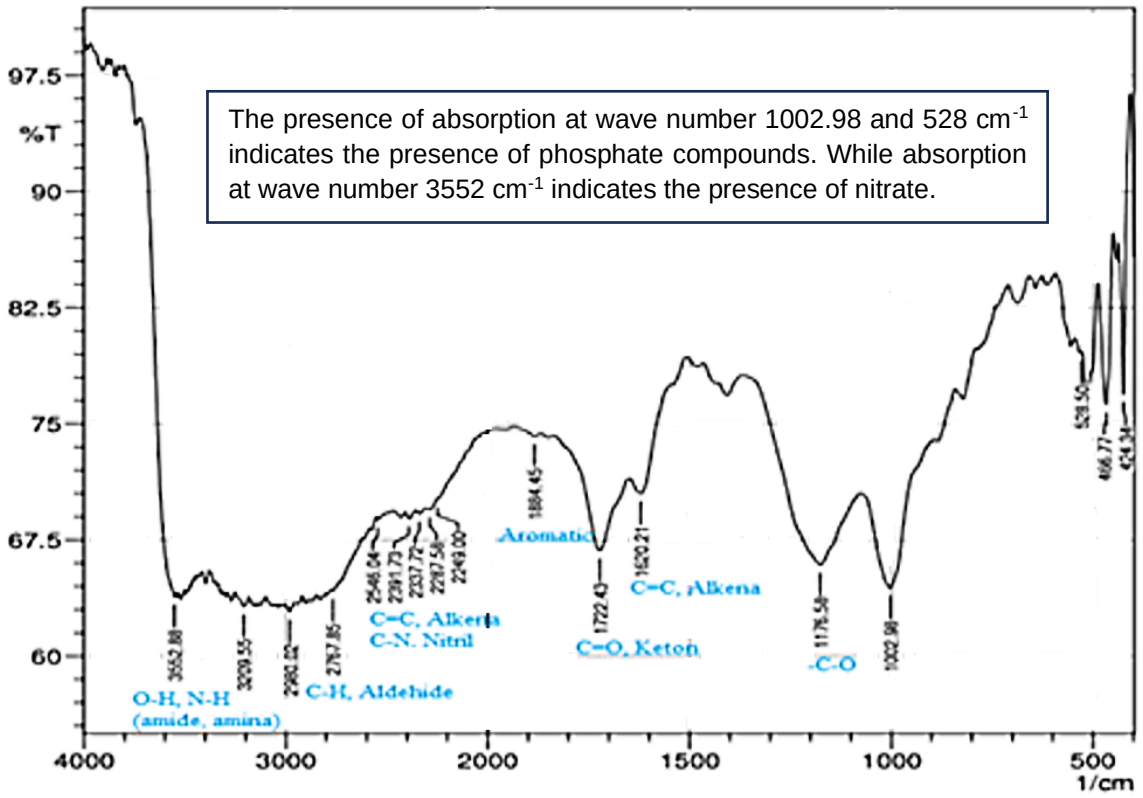

Figure 1. FTIR analysis of inhibitor.

Table 1. The elemental composition of the secondary pipes of RSG GAS

Fe	C	Si	Mn	Cr	Cu	Ni	S	P
99.52%	0.060%	0.004%	0.289%	0.17%	0.055%	0.24%	0.017%	0.008%

Analysis of Active Compounds in Inhibitors Using GCMS

The corrosion inhibitor compounds were analyzed using GCMS. The spectrogram data generated from the corrosion inhibitor yielded a fragmentation pattern, illustrated in Figure 2. The chromatogram data of the corrosion inhibitor unveiled various peaks. Major peaks in chromatograms with appropriate retention times: peaks at 5.685 minutes, 6.245 minutes, 6.685 minutes, main peak at 14.442 minutes, peaks at 14.773 minutes, 15.984 minutes, and 17.135 minutes. The highest peaks usually represent the compounds with the highest concentrations in the sample, but can also becaused by the high detector response to those compounds. Analysis of Dimethyl phosphonate Compound (RT 5.6878) - Found at a relatively small percentage, indicating a small presence in the sample. Chloromethyl thiocyanate (RT 6.1793) - Another minor component of the sample, with a low qualitative score. Ethane, 1,1,2,2-tetrachloro- (RT 6.2423) - Its moderate area percentage indicates that it is an important component of the inhibitor formulation. Trans-1-methyl-2-nonyl-cyclohexane (RT 6.6834) – present in smaller amounts compared to other compounds. 1H-Benzotriazole (RTs 14.4469 & 14.7746) - is a major corrosion inhibitor indicated by its high peak and area percentage. Table 2 Chemical compounds of inhibitor identified by GCMS.

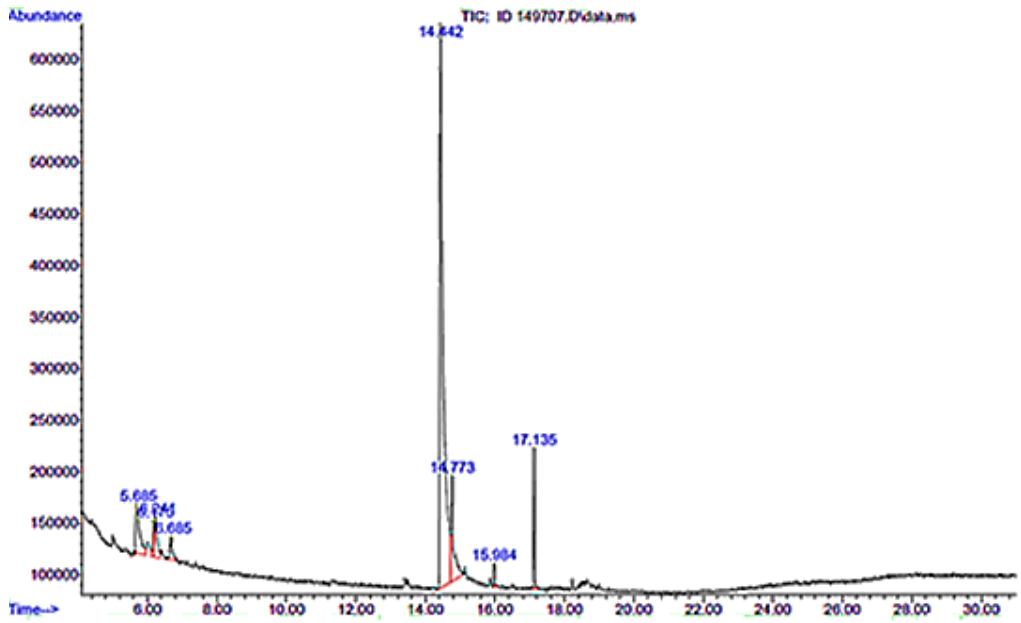

Figure 2. Spectrogram of analysis of corrosion inhibitor compounds was executed using GCMS.

Table 2. Chemical compounds of inhibitor identified by GCMS.

No	RT	Area Pct	Library/ID	Ref
1	5.6878	7.0346	Dimethyl methyl phosphonate	11723
2	6.1793	1.9311	Chloromethyl thiocyanate	5775
3	6.2423	3.5356	Ethane, 1,1,2,2-tetrachloro-	41600
4	6.6834	2.1512	Trans-1-methyl-2-nonyl-cyclohexane	104614
5	14.4469	70.1367	1H-Benzotriazole	10331
6	14.7746	10.1068	1H-Benzotriazole	10330
7	15.9845	0.7918	Tetradecane	74006
8	17.1313	4.3123	Heptadecane	123960

Ultrasonic-visible Analysis

Quantitative analysis of orthophosphate was carried out using an ultrasonic-visible spectrophotometer model carry 50, the orthophosphate concentration in the inhibitor was 4.2 ppm. this means that in 1000 mL of inhibitor there was 4.2 mg of phosphate

Visual Analysis

The outcomes of the analysis of AISI-1010 coupons submerged in secondary cooling water under two distinct treatments are illustrated in Figure 3. The AISI-1010 coupon subjected to immersion without an inhibitor (Fig. 3a) manifests a substantial corrosion process in contrast to the counterpart treated with an inhibitor (Fig. 3b). In the absence of a corrosion inhibitor, the metal surface becomes susceptible to the corrosive elements present in water, resulting in an accelerated oxidation process and material degradation. The corrosion phenomenon manifests through chemical reactions between the metal and environmental factors, such as oxygen and other corrosive agents within the water matrix. Conversely, introducing a corrosion inhibitor into water establishes a protective layer on the surface of AISI-1010, impeding or decelerating the corrosive reactions. This inhibitor creates a barrier that mitigates the interaction between the metal and the corrosive elements present in the water, thereby diminishing the corrosion rate. Consequently, the corrosion inhibitor acts as a preventive measure, augmenting the corrosion resistance of AISI-1010 and mitigating the adverse effects of exposure to the aqueous environment.

 DOI: https://doi.org/10.55981/Urania.2025.8674

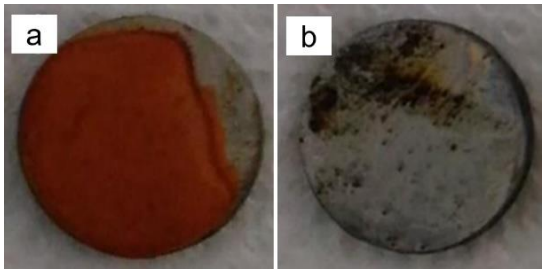

Figure 3. Visual observation of AISI-1010 carbon steel, immersion without inhibitor (a); and with inhibitor (b).

SEM Analysis

The scanning electron microscope (SEM) test is employed to scrutinize the surface morphology of materials [10], [13], [15]. In this study, the SEM test was conducted on two distinct samples: AISI-1010 specimens without inhibitors and AISI-1010 specimens with inhibitors. The outcomes of the SEM test are depicted in Figure 4 and Figure 5. In Figure 4, the SEM test results for AISI 1010 without inhibitors are presented, 4a. an image magnified 100x and 4b an image magnified 500x, involving an initial pickling process to cleanse corrosion products resulting from interaction with ambient air using an HCl solution. Figure 4(a) presents the surface material with inhibitor that an image magnified at 100X, revealing minor porosity on the surface of AISI-1010. In contrast, Figure 4(b) depicts an image magnified at 500X, showcasing spheroidal circles attributed to the pickling process. The surface of AISI 1010, as observed with SEM, indicates the presence of a base material image with porosity, magnifying into a spheroid. This spheroidal formation facilitates interaction with oxygen, rendering the material susceptible to corrosion.

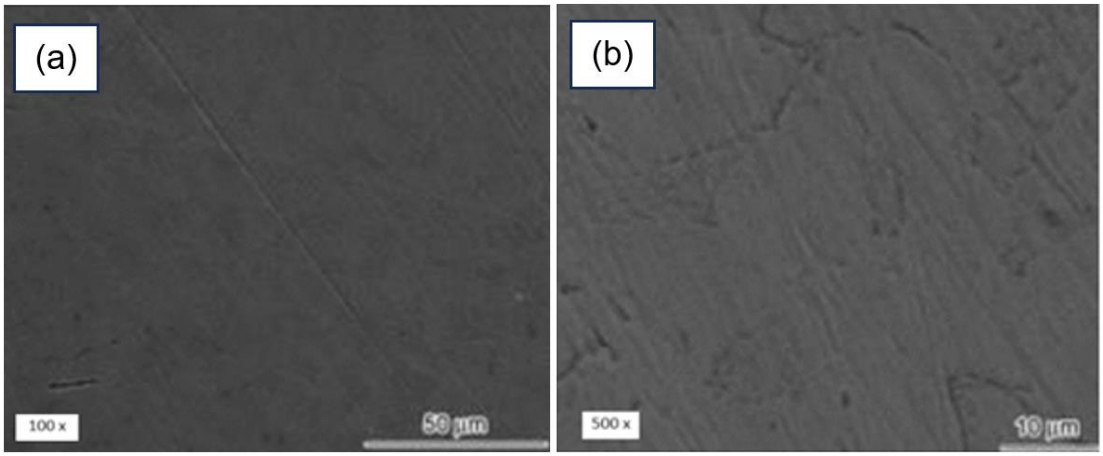

Figure 4. SEM images of AISI-1010 material in without the inhibitors.

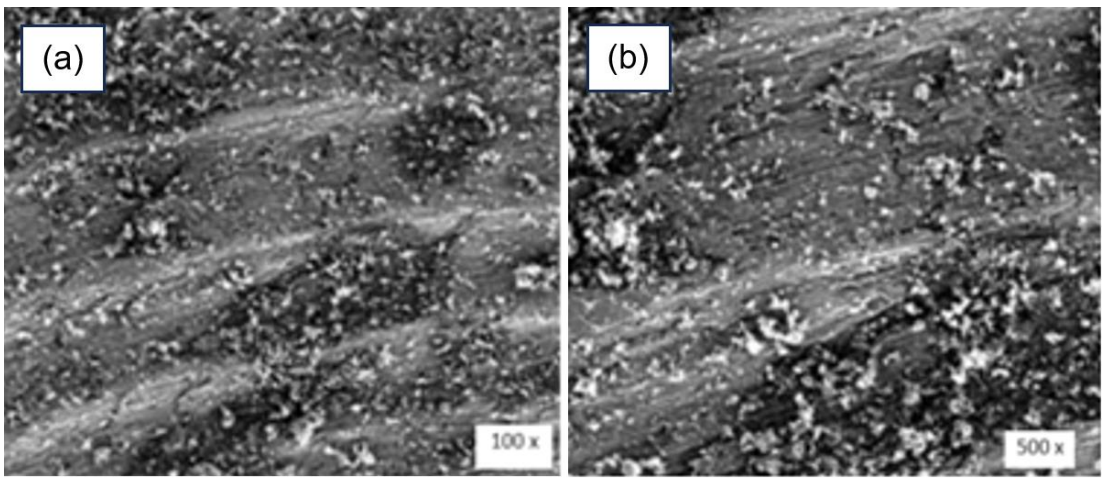

Figure 5. SEM images of AISI-1010 material treated with an inhibitor.

The micrographs in Figure 5 taken at magnifications of 100X and 500X, it is apparent that a uniform protective film envelops the surface morphology. No traces of corrosion products are observable on the AISI-1010 surface. Therefore, it can be deduced that the inhibitor, which contains zinc phosphate as its active component, establishes a protective coating on the surface of AISI-1010. This protective coating effectively masks surface porosity, thereby hindering oxidative corrosion [32],[33].

AISI-1010 Corrosion Test

The corrosion assessment of AISI-1010 material was conducted utilizing the EG&G Potentiostat/Galvanostat Model 273. The test medium employed was secondary cooling water, with and without the addition of inhibitors at concentrations ranging from 75, 100, to 150 ppm. The Tafel polarization technique was applied for the analysis of the corrosion rate [34]. The outcomes of the Tafel analysis are depicted in Figure 6, accompanied by the corresponding corrosion rate values presented in Table 3.

The data depicted in Figure 6 elucidates that the inclusion of the inhibitor, within the range of 0 to 100 ppm, induces a shift in the polarization curve towards the cathodic direction. Conversely, the inclusion of the inhibitor at a concentration of 150 ppm manifests a shift in the curve toward the anodic direction. Consequently, it can be deduced that the inhibitor system functions as a mixed-type inhibitor [35].

Table 3. The corrosion rate of AISI-1010 specimens in the secondary water of RSG-GAS, with and without inhibitor.

Inhibitor conc. (ppm)	E_{corr} (mV)	I_{corr} (10^{-2} µA/cm^2)	CR (mpy)	IE (%)
0	-588.97	12.83	10.96	-
75	-562.48	14.86	7.21	34.21
100	-565.54	15.70	6.93	36.77
150	-570.73	23.78	5.84	46.71

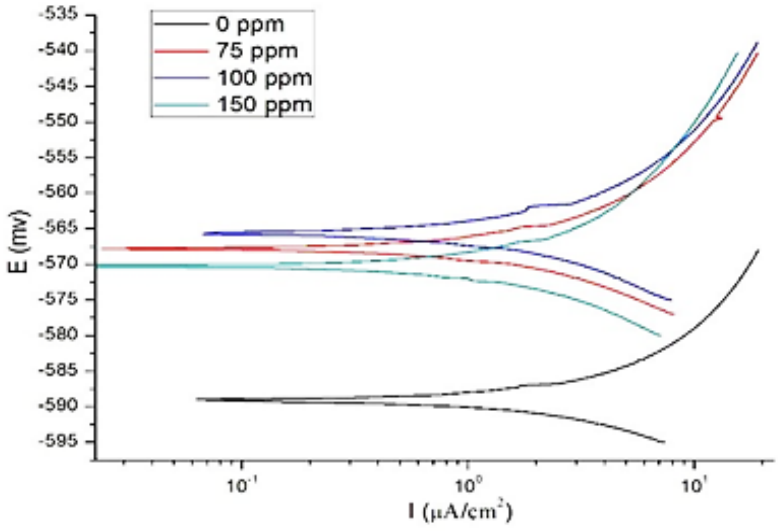

Figure 6. Tafel polarization curves for AISI 1010 in secondary cooling water with inhibitor concentrations of 0 ppm, 50 ppm, 100 ppm, and 150 ppm.

The corrosion rate of AISI 1010 was deduced based on the corrosion current (I_{Corr}) and E_{Corr} observed during the experiment, as elaborated in Table 3. Both Icorr and Ecorr values were derived from Tafel polarization analysis. Compared to samples without inhibitors, the E_{Corr} of inhibitor samples is higher. A higher resistance to corrosion attacks is indicated by E_{Corr} values that are positive or larger. The maximum corrosion

 DOI: https://doi.org/10.55981/Urania.2025.8674

rate was observed in materials immersed without an inhibitor, recorded at 10.96 mpy. In contrast, the minimum corrosion rate was noted in materials submerged in RSG-GAS secondary cooling water with the addition of an inhibitor, measuring 5.84 mpy. The trend dependent on concentration suggests that higher inhibitor concentrations reduce corrosion rates for AISI-1010 carbon steel. The inhibitor concentration of 150 ppm is deemed optimal due to its economic viability and its capability to functionally impede the corrosion process by 46.71%.

The outcomes of the polarization test for each material are derived from diverse parameters, including Ecorr and Icorr, as depicted in Table 3 based on the polarization test results. Figure 7 illustrates that as the concentration of the corrosion inhibitor increases, there is a corresponding decrease in the corrosion rate observed in the AISI-1010 material. By adhering to the surface, the inhibitor present in the solution prevents aggressive ions from penetrating the secondary water at the AISI-1010 steel aperture. Numerous investigations demonstrate a somewhat similar finding, namely that the rate of corrosion can be decreased if a substance inhibits the sample's surface[36].

The Langmuir Adsorption Isotherm theory is employed to discern the interaction between the inhibitor and the material surface [37][38][39]. Utilizing Langmuir's calculations, this methodology elucidates the adsorption phenomenon occurring on the material surface, enabling the determination of whether the reaction is in the form of physisorption or chemisorption. Through calculations based on the Langmuir adsorption isotherm, crucial parameters such as surface coverage values, K_{ads} and G_{ads} are obtained. These calculations yield insights into the extent of adsorption on corrosion inhibitors across various concentrations. The comprehensive adsorption-free energy values are presented in Table 4.

The determination of the adsorption method on the material surface can be inferred from the value of Gads. Following Singh's guidelines (2012), if the Gads value surpasses -20 kJ/mol, the formed adsorption process is categorized as physisorption. In cases where Gads fall between -20 to -40 kJ/mol, the adsorption process is considered a mixed mechanism involving both physisorption and chemisorption. Conversely, when the Gads value is more negative than -40 kJ/mol, it indicates the prevalence of a chemisorption process. In the dataset derived from scale corrosion inhibitors, the Gads value exceeds -20 kJ/mol, signifying that the adsorption method between the material surface and the inhibitor is predominantly a physisorption process [39].

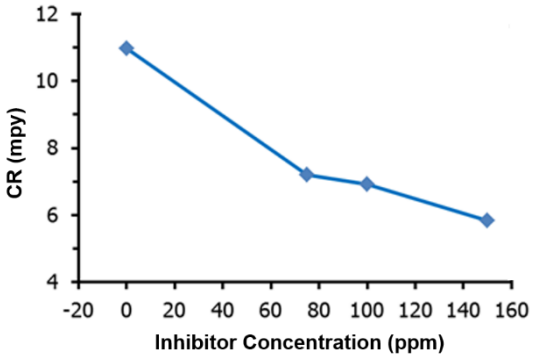

Figure 7. The corrosion rate graph of AISI 1010 in the secondary cooling system with varying concentrations of corrosion inhibitors: 0 ppm, 75 ppm, 100 ppm, and 150 ppm.

Table 4. Free energy adsorption on crust inhibitor corrosion.

Inhibitor concentration (ppm)	Surface coverage (θ)	K_{ads}	G_{ads}(kJ/mol)
75	0.341	0.00683	2.402
100	0.367	0.00562	2.886
150	0.467	0.00549	2.940

Characterization of inhibitors was carried out using FTIR and GCMS, and analysis of orthophosphate levels in inhibitors was also carried out using UV-Vis spectroscopy, with results showing orthophosphate levels of 4.2 ppm. The presence of orthophosphate as an active component in the inhibitor plays an important role in forming a passive layer on the surface of AISI-1010 material. Orthophosphate is known to have the ability to

create complex compounds with Fe ions on metal surfaces, forming a protective layer that prevents direct interaction between metal surfaces and corrosive agents.

The content of orthophosphate in the inhibitor solution can function as an anodic inhibitor, where orthophosphate plays a role in blocking oxidation reactions in anodic areas on metal surfaces. In this study, the concentration of orthophosphate of 4.2 ppm can be said to be quite significant, although it is relatively lower than the concentration commonly used in commercial inhibitors. These results provide additional perspective regarding the effectiveness of inhibitors used at specific concentrations and specific operating environments in RSG-GAS secondary cooling systems. The effectiveness of orthophosphate in lowering corrosion rates by up to 46.71% indicates that although the inhibition rate is not high, orthophosphate contributes to a substantial increase in corrosion resistance compared to conditions without inhibitors. Our results indicate the importance of orthophosphate levels in mitigating the corrosion effects of AISI-1010 materials and provide potential early insights for the development of more effective inhibitors.

CONCLUSIONS

The introduction of a corrosion inhibitor into the secondary cooling system of the RSG-GAS constitutes a preventive measure against the corrosion process. Elemental testing has confirmed that the material for the RSG-GAS secondary pipes is AISI-1010. When a corrosion inhibitor is introduced into the coolant at a concentration of 150 ppm, the AISI-1010 carbon steel material demonstrates enhanced corrosion resistance. There is a notable reduction in the measured corrosion rate by 46.71%, decreasing from 10.96 mpy to 5.84 mpy. The inhibitor layer effectively conceals porosity on the surface of AISI-1010, as observed in the SEM test results. Analysis of the polarization curve direction indicates that the corrosion inhibitor operates as a mixed-type inhibitor. Notably, visual inspection reveals the absence of corrosion products on the AISI-1010 layer immersed in the inhibitor solution, whereas visible corrosion products are evident on the material lacking inhibitors.

ACKNOWLEDGEMENT

This research is underwritten and financially supported by the RIIM-Batch 4 BRIN, Nomor 37/II.7/HK/2023 allocation for the fiscal year 2023. The authors extend their sincere appreciation for the financial backing and laboratory amenities bestowed upon this research.

AUTHOR CONTRIBUTIONS

All researchers who are involved are the main contributors.

REFERENCES

[1]. E. Ratnawati, D. E. Lestari, and T. R. Mulyaningsih, “Studi pengotor pada pendingin primer reaktor RSG-GAS setelah 30 tahun beroperasi, *Ganendra Maj. IPTEK Nukl*., vol. 21, no. 1, 2018, doi: 10.17146/gnd.2018.21.1.3675.

[2]. S. Sriyono et al., “The debris particles analysis of RSG-GAS coolant to anticipate sediment induced corrosion,” *J. Pengemb. Energi Nukl*., vol. 18, no. 1, 2016. doi: 10.17146/jpen.2016.18.1.2675.

[3]. G. R. Sunaryo, M. I. Santoso, and R. Kusumastuti, “An in-depth four-year investigation into corrosion of carbon steel materials in the secondary cooling piping of the 30 MW RSG-GAS research reactor,” Int. J. Corrosion.Scale Inhib., vol. 13, no. 2, pp. 853–873, 2024, doi: 10.17675/2305-6894-2024-13-2-11.

[4]. G. R. Sunaryo, “Surveillance management for secondary water cooling quality of RSG-GAS,” *J. Sains dan Teknol. Nukl. Indones*., 2017, doi: 10.17146/jstni.2017.18.1.3214.

[5]. R. Kusumastuti, D. Erlina Lestari, G. Rina Sunaryo, “Water Chemistry Analysis In RSG-GAS Secondary Cooling System,” 2016.

[6]. S. D. Lee, S. R. Mallampati, and B. H. Lee, “Enhanced removal of ethanolamine from secondary system of nuclear power plant wastewater by novel hybrid nano zero-valent iron and pressurized ozone initiated oxidation process,” *Environ. Sci. Pollut. Res*., vol. 24, no. 21, pp. 17769–17778, 2017, doi: 10.1007/s11356-017-9416-4.

[7]. J. I. Malik, N. M. Mirza, and S. M. Mirza, “Simulation of corrosion product activity in extended operating cycles of PWRs

under flow rate transient and nonlinearly rising corrosion rates coupled with pH effects," *Nucl. Eng. Des*., vol. 249, pp. 388–399, 2012, doi: 10.1016/j.nucengdes.2012.04.013.

[8]. J. Huang, D. Lister, S. Uchida, and L. Liu, "The corrosion of aluminium alloy and release of intermetallic particles in nuclear reactor emergency core coolant: Implications for clogging of sump strainers," *Nucl. Eng. Technol.,* vol. 51, no. 5, pp. 1345–1354, 2019, doi: 10.1016/j.net.2019.02.012.

[9]. M. Jobst, P. Wilhelm, Y. Kozmenkov, and S. Kliem, "Severe accident management measures for a generic German PWR. Part II: Small-break loss-of-coolant accident," *Ann. Nucl. Energy*, vol. 122, pp. 280–296, 2018, doi: 10.1016/j.anucene.2018.08.017.

[10]. P. Pla, F. Reventos, M. Martin Ramos, I. Sol, and M. Strucic, "Simulation of steam generator plugging tubes in a PWR to analyze the operating impact," *Nucl. Eng. Des*., vol. 305, pp. 132–145, 2016, doi: 10.1016/j.nucengdes.2016.05.002.

[11]. M. Slobodyan, "High-energy surface processing of zirconium alloys for fuel claddings of water-cooled nuclear reactors," *Nucl. Eng. Des*., vol. 382, no. July, p. 111364, 2021, doi: 10.1016/j.nucengdes.2021.111364.

[12]. P. M. Udiyani, S. Kuntjoro, G. R. Sunaryo, and H. Susiati, "Atmospheric dispersion analysis for expected radiation dose due to normal operation of RSG-GAS and RDE reactors," *Atom Indones.*, vol. 44, no. 3, pp. 115–121, 2018, doi: 10.17146/aij.2018.878.

[13]. C. H. Pyeon, T. Endo, G. Chiba, K. Watanabe, and G. Wakabayashi, "Nuclear education programs with reactor laboratory experiments at zero-powered research reactor facilities in Japan," *Ann. Nucl. Energy*, vol. 204, no. February, p. 110531, 2024, doi: 10.1016/j.anucene.2024.110531.

[14]. M. Al-dbissi, I. Pázsit, R. Rossa, A. Borella, and P. Vinai, "On the use of neutron flux gradient with ANNs for the detection of diverted spent nuclear fuel," *Ann. Nucl. Energy*, vol. 204, no. March, p. 110536, 2024, doi: 10.1016/j.anucene.2024.110536.

[15]. P. Suganya, et al., "Assessing the factors affecting the water chemistry parameters in the auxiliary water system of a nuclear power plant," *SN Appl. Sci*., vol. 2, no. 11, pp. 1–13, 2020, doi: 10.1007/s42452-020-03693-z.

[16]. S. Setiawati, H. Alikodra, B. Pramudya, and A. H. Dharmawan, "Model of Water, Energy and Waste Management for Development of Eco-Innovation Park ; A Case Study of Center for Research of Science and Technology 'PUSPIPTEK,' South Tangerang City, Indonesia," *World Technop. Rev*., vol. 3, no. 2, pp. 89–96, 2014, doi: 10.7165/wtr2014.3.2.89.

[17]. S. Q. Feng Yang; Xiangyu Li, "Water_Solubility."Int.J.Electrochem.Sci, pp. 5349–5362, 2017.

[18]. W. Xie, J. Li, and Y. Li, "Electrochemical corrosion behavior of carbon steel and hot dip galvanized steel in simulated concrete solution with different pH values," *Medziagotyra*, vol. 23, no. 3, pp. 280–284, 2017, doi: 10.5755/j01.ms.23.3.16675.

[19]. Z. Moallem, I. Danaee, and H. Eskandari, "Corrosion Inhibition and Adsorption Behavior of Gentian Violet on AISI 4130 Alloy Steel in HCl Solution," *Trans. Indian Inst. Met.,* vol. 67, no. 6, pp. 817–825, 2014, doi: 10.1007/s12666-014-0403-x.

[20]. A. Fawzy, et al, "Thermodynamic, kinetic and mechanistic approach to the corrosion inhibition of carbon steel by new synthesized amino acids-based surfactants as green inhibitors in neutral and alkaline aqueous media," J*. Mol. Liq*., vol. 265, pp. 276–291, Sep. 2018, doi: 10.1016/j.molliq.2018.05.140.

[21]. Z. Yao, D. Wang, N. Xu, C. Du, Y. Feng, and Y. Qi, "Phosphate and humic acid inhibit corrosion of green-synthesized nano-iron particles to remove Cr(VI) and facilitate their cotransport," *Chem. Eng. J*., vol. 450, p. 136415, Dec. 2022, doi: 10.1016/j.cej.2022.136415.

[22]. R. Kusumastuti, R. I. Pramana, and J. W. Soedarsono, "The use of morinda citrifolia as a green corrosion inhibitor for low carbon steel in 3.5% NaCl solution," 2017, p. 020012. doi: 10.1063/1.4978085.

[23]. R. I. Pramana, R. Kusumastuti, J. W. Soedarsono, and A. Rustandi, "Corrosion Inhibition of Low Carbon Steel

by Pluchea Indica Less. in 3.5% NaCL Solution," *Adv. Mater. Res.,* vol. 785–786, pp. 20–24, 2013, doi: 10.4028/www.scientific.net/AMR.785-786.20.

[24]. W. Zhang, et al., "Aloe polysaccharide as an eco-friendly corrosion inhibitor for mild steel in simulated acidic oilfield water: Experimental and theoretical approaches," *J. Mol. Liq*., vol. 307, 2020, doi: 10.1016/j.molliq.2020.112950.

[25]. M. Keramatinia, B. Ramezanzadeh, and M. Mahdavian, "Green production of bioactive components from herbal origins through one-pot oxidation/polymerization reactions and application as a corrosion inhibitor for mild steel in HCl solution," *J. Taiwan Inst. Chem. Eng.,* vol. 105, pp. 134–149, 2019, doi: 10.1016/j.jtice.2019.10.005.

[26]. G. A. Gaber, et al., "A computational and experimental investigation of novel synthesis fused pyrazolopyrimidine as zinc corrosion inhibitor in 1 M HNO3," *Chem. Pap.,* vol. 78, no. 5, pp. 3189–3203, 2024, doi: 10.1007/s11696-024-03303-x.

[27]. B. A. Abd-El-Nabey, S. El-Housseiny, and M. A. Abd-El-Fatah, "Improved corrosion resistance of permanganate-phosphate conversion coat on steel surface by surfactants," *Sci. Rep.,* vol. 13, no. 1, pp. 1–20, 2023, doi: 10.1038/s41598-023-41394-w.

[28]. E. R. Safitra, "Studi sistem injeksi inhibitor korosi terhadap kandungan orthofosfat dan seng sebagai parameter kendali korosi pada sistem pendingin sekunder RSG-GAS." *Journal of Science and Applicative Technology*, 2018.

[29]. S. L. Butarbutar and G. R. Sunaryo, "Analisis mekanisme pengaruh inhibitor siskem pada material baja karbon," *Pros. Semin. Nas. ke-17 Teknol. dan Keselam. PLTN Serta Fasilitas Nukl*., 2011.

[30]. A. A. Aguilar-Ruiz, et al., "Effectiveness of green coatings as a possible protection barrier against corrosion," *MRS Adv*., vol. 9, no. 4, pp. 193–198, 2023, doi: 10.1557/s43580-023-00728-6.

[31]. S. C. Ikpeseni et al., "Electrochemical and adsorption studies of siam leaf extract's effect on mild steel corrosion inhibition in sulphuric acid medium," *J. Bio- Tribo-Corrosion*, vol. 10, no. 3, pp. 1–11, 2024, doi: 10.1007/s40735-024-00845-1.

[32]. S. Ding et al., "Effect of phosphorus modulation in iron single-atom catalysts for peroxidase mimicking," *Adv. Mater.*, vol. 36, no. 10, 2024, doi: 10.1002/adma.202209633.

[33]. L. Yohai, M. Vázquez, and M. B. Valcarce, "Phosphate ions as corrosion inhibitors for reinforcement steel in chloride-rich environments*," Electrochim. Acta*, vol. 102, pp. 88–96, Jul. 2013, doi: 10.1016/j.electacta.2013.03.180.

[34]. D. M. Bastidas, et al., "Comparative study of three sodium phosphates as corrosion inhibitors for steel reinforcements," *Cem. Concr. Compos*., vol. 43, pp. 31–38, 2013, doi: 10.1016/j.cemconcomp.2013.06.005.

[35]. X. Zhang, et al., "Epiberberine: a potential rumen microbial urease inhibitor to reduce ammonia release screened by targeting UreG," *Appl. Microbiol. Biotechnol.*, vol. 108, no. 1, 2024, doi: 10.1007/s00253-024-13131-4.

[36]. A. Hern·ndez-Espejel, et al., "Investigations of corrosion films formed on API-X52 pipeline steel in acid sour media," *Corros. Sci*., vol. 52, no. 7, pp. 2258–2267, 2010.

[37]. A. Nikitasari et al., "Anti-corrosion inhibition of API 5L in hydrochloric acid solution by ethanol extract of Phyllanthus niruri leaf," *Int. J. Corros. Scale Inhib*., vol. 13, no. 1, pp. 1–20, 2024, doi: 10.17675/2305-6894-2024-13-1-1.

[38]. M. A. Deyab et al., "Synthesis, surface activity, and corrosion inhibition capabilities of new non-ionic gemini surfactants," *Sci. Rep*., vol. 14, no. 1, pp. 1–15, 2024, doi: 10.1038/s41598-024-57853-x.

[39]. X. Wang, Z. Chen, C. Wang, and L. Zhang, "Ultrahigh and kinetic-favorable adsorption for recycling urea using corncob-derived porous biochar," *Sci. Rep.*, vol. 14, no. 1, pp. 1–17, 2024, doi: 10.1038/s41598-024-58538-1.